Chemical Engineering Science 309 (2025) 121469

Contents lists available at ScienceDirect

Chemical Engineering Science

journal homepage: www.elsevier.com/locate/ces

Particle size segregation in bi and penta-disperse gas–solid fluidized beds: CFD-DEM and recurrence CFD simulations

S. Pirker [a,*], M. Atzori [b], S. Heinrich [c], T. Lichtenegger [a,b]

[a] Department of Particulate Flow Modelling, Johannes Kepler University Linz, Austria
[b] Deptartment of Aerospace Engineering, Politecnico di Milano, Italy
[c] Institut of Solids Process Engineering, Technical University Hamburg, Germany

ARTICLE INFO

Keywords:
Recurrence CFD
Fluidized beds
Segregation
Granulation process

ABSTRACT

We studied the time evolution of segregating particle fractions in gas–solid fluidized beds by unresolved CFD-DEM and data-based recurrence CFD (rCFD).

First and foremost, we incorporated segregating particle fractions into rCFD by superposing a fractional drift velocity to the velocity of the solid bulk material. From an algorithmic viewpoint, fractional drift was implemented by discrete face swaps. We tested this novel rCFD approach with different superficial gas velocities and different bi-disperse bed inventories. rCFD predictions agreed very well with corresponding full CFD-DEM results with respect to the time-evolution of fractional centre-of-gravity as well as spatial line profiles of fractional mean volume fraction.

In order to explore the validity range of the underlying databases, we intentionally ran rCFD at deviating conditions. In a first test, we showed that rCFD simulations could indicate regime-changing de-fluidization even if de-fluidization itself was not pictured in the database. In a second test, we performed penta-disperse rCFD simulations based on an equivalent bi-disperse database. Hereby, we found out that rCFD predictions were only accurate if the penta-disperse bed inventory did not lead to changing overall bed dynamics. Finally, we proved the feasibility of rCFD simulations of a granulation process featuring local particle growth as well as continuous feed input and product output.

In all cases, rCFD simulations ran more than four orders of magnitude faster than corresponding CFD-DEM simulations, eventually allowing for real-time simulations of spatially resolved particle segregation in fluidized beds.

1. Introduction

Bubbling gas–solid fluidized beds are widely used in process industries due to the intense contact between solid particles and the agitating gas phase, which enables very efficient particle mixing as well as gas–solid heat and mass transfer (Chew et al., 2022). In granulation processes, fluidized beds are employed to expose solid particles to a liquid spray zone, where solid particles receive portions of liquid which are subsequently dried and solidified by efficient gas contact (Zafiryadis et al., 2023).

Granulation processes are inherently poly-disperse since they rely on local particle growth. In fluidized beds, any disperse distribution of solid particles – either by size or density – can give rise to the physical phenomenon of segregation, describing the de-mixing of individual particle fractions (Dahl & Hrenya, 2005; Rowe & Nienow, 1976; Wu & Baeyens, 1998). In bubbling fluidized beds, size-dependent segregation of particles with the same particle density is triggered by the gas–solid drag force, which entails that larger particles accumulate in the lower part of the fluidized bed while smaller particles are more likely encountered in the upper part. Wide particle size distributions (PSDs) might deteriorate fluidized bed operations such that very large particles just reside on the bottom of the bed while very small particles are actually washed out of the bed by the gas stream. In extreme cases, immobile large particles might lead to blockage of the gas entry, causing de-fluidization and eventually a breakdown of the whole process. While this dramatic effect of segregation should certainly be avoided, mild segregation could even be used to produce a more homogeneous bed inventory, by intentionally aligning the particle growth zone with the region of smaller particles

* Corresponding author.
E-mail address: stefan.pirker@jku.at (S. Pirker).

https://doi.org/10.1016/j.ces.2025.121469
Received 23 December 2024; Received in revised form 12 February 2025; Accepted 1 March 2025
Available online 2 March 2025

(Atxutegi et al., 2024).

For any of the two motivations – avoiding de-fluidization or optimizing the particle growth zone – a sound understanding of segregation in fluidized beds is on need.

Naturally, any investigation method in this regard requires the assessment of particle size distribution. Experimentally, the effect of segregation in bubbling fluidized beds has been studied by instantaneously switching off the gas supply and subsequently investigating the layered PSDs of the post-mortem fluidized bed (Joseph et al., 2007). In a less invasive mode, PSDs have also been obtained by point probing the bed inventory (Wiegel et al., 2016). In recent years, several groups tried to assess time-dependent segregation in quasi two-dimensional fluidized beds by Digital Image Analysis (DIA), employing particle fractions of different colors (de Munck et al., 2023; Jiang et al., 2018; Olaofe et al., 2013). Interestingly, these studies indicate that particle segregation has to be regarded as an unsteady process which slowly evolves on top of the fast bed dynamics.

Obviously, numerical simulations represent an alternative approach to shed light on the detailed three-dimensional behavior of bubbling fluidized beds. By applying particle-based Discrete Element Method (DEM) simulations a poly-disperse bed inventory can be resolved and the time-evolving process of segregation can be shown (Fries et al., 2011). However, since the process of segregation is slow compared to the overall bed dynamics, such long-term DEM simulations require a lot of computational resources and therefore are typically restricted to lab-scale fluidized beds.

Several numerical methods exist which aim to reduce the computational costs of particle-based DEM simulations. Most prominently, Two-Fluid Models (TFM) smear out individual particles into an artificial solid phase which interacts with the interstitial gas phase by e.g. momentum transfer. However, in case of poly-disperse particle ensembles, classical TFM simulations would require a complete set of transport equations for each individual particle fraction which again becomes very expensive. One of the authors has also tried to address segregation in bubbling fluidized beds by a hybrid combination of TFM and poly-disperse Lagrangian tracers (Schneiderbauer et al., 2015). Although that study could reproduce macroscopic segregation effects, the applied hybrid model suffers from insufficiently addressed physics (e.g. by neglecting particle rotation or inter-particle friction).

In this paper, we will try to reduce computational costs by the concept of recurrence CFD (rCFD) (Lichtenegger & Pirker, 2016), which relies on the recurrent nature of bubbling fluidized beds. Essentially, rCFD is a two phase data-assisted method, which in a first phase collects data from conventional simulations before they are time extrapolated in a second phase. For the purpose of data collection, classical particle-based CFD-DEM simulations are performed for only a short duration of time. From these expensive simulations a database is deduced which in a second phase enables the fast propagation of passive scalars for longer time-spans. While Lichtenegger et al. (2017) applied rCFD to picture the time-evolution of particle temperature fields in a bubbling fluidized bed, Kieckhefen et al. (2019) studied the process of particle coating in a spout fluidized bed. Lichtenegger et al. (2019) further advanced the rCFD representation of bubbling fluidized bed by interpolating between two databases, thus allowing for changing process conditions. In all cases, computational times could be reduced drastically by two to three orders of magnitude.

In another transport-based version of rCFD, convection and diffusion of passive scalars are not solved anymore by dedicated transport equations but are represented by pre-determined cell-to-cell shifts and face swaps. Employing such discretized Lagrangian propagators, Pirker and Lichtenegger (2018) successfully reproduced heat transfer in a bubbling fluidized bed while Dabbagh et al. (2020) addressed poly-olefine production processes. This discretized mode of information transport turned out to be even more performant allowing for speed-ups in the order of (more than) four orders of magnitude.

To our best knowledge, rCFD has never been applied to poly-disperse fluidized beds. In the current paper, we therefore and foremost aim to explore the feasibility of implementing segregating particle fractions into transport-based rCFD simulations of bubbling fluidized beds. In order to assess the new model's predictive capabilities, we compare numerical prediction of rCFD simulations to corresponding particle-based CFD-DEM reference simulations.

Beyond proving its pure feasibility, we will question in how far rCFD simulations can tolerate deviations from the underlying database, which might occur e.g. due to changes in the flow regime or by varying solid inventories. In a first test, we explore if rCFD simulations can provide indications of potential de-fluidization even if the (regime changing) de-fluidization is not pictured in the database. In a second test, we ask whether rCFD simulations can represent time-evolving patterns of particle size distributions even if the actual bed inventory differs from that used for the generation of the database. By thoroughly assessing rCFD's predictive capabilities, we will identify limits of database deviations. Finally, we will prove the feasibility of rCFD simulations of a granulation chamber featuring particle growth as well as continuous particle through-flow.

In the next Section 2 we focus on how drag-induced particle segregation can be introduced in the algorithmic environment of transport-based rCFD. In the following Section 3, we first present results of incipient segregation for bi-disperse particle ensembles. This is followed by a study on database-deviating rCFD simulations focusing on de-fluidization and poly-dispersity before a last subsection proves the feasibility of simulating a granulation chamber. In Section 4 we conclude our work and provide an outlook.

2. Modelling

2.1. Conventional unresolved CFD-DEM simulations

In the course of this study we performed two sets of conventional CFD-DEM simulations. While the first set of short-term simulations was used for the creation of dedicated databases for subsequent rCFD simulations, a second set of CFD-DEM reference simulations served as validation base (numerical ground-truth) for the numerical predictions of the rCFD simulations.

Essentially, standard CFD-DEM modelling was applied within the software framework of CFDEMcoupling_PFM (2024). The computational domain resembles a rectangular fluidized bed of $L \times D \times H = 0.2 \times 0.05 \times 0.7[m]$, which was discretized by a Eulerian grid of 60 k hexahedral cells. Depending on the degree of poly-dispersity, the solid inventory was represented by (up to) 350 k discrete particles, which resulted in typical computational time of (up to) 22 h for one second of real-world process time.

Upon initialization, particles were randomly arranged in a loosely packed column, which subsequently collapsed to the bottom of the bed at the start of each simulation. After that the upward gas stream governed the macroscopic particle pattern by Beetstra momentum exchange. Further modelling details of these conventional CFD-DEM simulations are given in Atxutegi et al. (2024). For the sake of completeness, a set of model parameters is provided in Table 1.

A summary of all simulated cases is given in Table 2 with the considered bi- and penta-disperse particle populations detailed in Table 3. Note that we intentionally opted for very low superficial velocities of $u = 1.1(1.2)\ m/s$ because particle size segregation is expected to be more significant at low bath agitation.

2.2. Recurrence CFD simulations

The rCFD simulations rely purely on pre-calculated field information of the solid phase (e.g. particle velocities or particle displacement mapped onto a Eulerian grid), and the gas flow obtained with a higher fidelity method (standard CFD-DEM simulations, in our case). Additional modelling, for instance related to the inter-phase drag, is not

Table 1
Setup of the simulation for (top) OpenFOAM and (bottom) LIGGGHTS. Material properties are the same as the in study by Diez et al. (2019).

Number of cells	80,000
$\Delta x = \Delta y = \Delta z$ [mm]	5
Δt_{CFD} [s]	2.5·10−5
ρ [kg/m^3]	1.189
ν [m^2/s]	$10-5$
Number of particles (depending on population)	90000–350000
Particle Sauter diameters [mm]	1.412
Δt_{DEM} [s]	$2.5 \cdot 10-6$
ρ [kg/m3]	1440
u_{mf} [m/s]	1.1, 1.2
Young modulus [GPa] (particle, wall)	1.58, 1.80
Poisson ratio (particles, wall)	0.22, 0.3
COR (particle–particle, particle–wall)	0.55, 0.55
Sliding friction coeff. (particle–particle)	0.8693
Sliding friction coeff. (particle–wall)	0.0981

Table 2
List of CFD-DEM simulations; note that databases were extracted from only the top four simulations while the others just served for the purpose of numerical validation; all simulations were run for five seconds real-world time except for the long ones which covered 20 s, particle populations are further detailed in Table 3.

Case name	u_{sup} [m/s]	population
fb_u1.1_biN	1.1	bi-narrow
fb_u1.2_biN	1.2	bi-narrow
fb_u1.1_biW	1.1	bi-wide
fb_u1.2_biW	1.2	bi-wide
fb_u1.1_pentaN	1.1	penta-narrow
fb_u1.2_pentaN	1.2	penta-narrow
fb_u1.1_pentaW	1.1	penta-wide
fb_u1.2_pentaW	1.2	penta-wide
fb_u1.1_biN_long	1.1	bi-narrow
fb_u1.2_biN_long	1.2	bi-narrow
fb_u1.1_biW_long	1.1	bi-wide
fb_u1.2_biW_long	1.2	bi-wide

Table 3
List of particle populations, individual particle fractions are defined by doublets of diameter [m] and mass fraction [kg/kg], note that all populations share the same Sauter mean diameter of $d_{32} = 2.284$mm.

Population	d_i [mm]/mf_i [.]		
bi-narrow	1.950/0.473	2.820/0.527	
bi-wide	1.459/0.564	4.075/0.437	
penta-narrow	1.783/0.100	1.998/0.205	2.284/0.445
	2.855/0.150	3.426/0.100	
penta-wide	1.141/0.100	1.713/0.123	2.284/0.427
	3.426/0.200	4.568/0.150	

required at this level.

As with standard CFD-DEM, we abstain from a detailed description of the main functionality of the transport-based recurrence CFD method, since it has been presented in great detail elsewhere (Pirker & Lichtenegger, 2018). In the next subsections, we rather focus solely on the novel functionality of segregating particle fractions.

2.2.1. Segregating particle fractions

In a data-preparation phase, we performed conventional bi-disperse CFD-DEM simulation, such that the Sauter mean diameter $d_{32} = \sum_i N_i d_i^3 / \sum_i N_i d_i^2$ of the original solid inventory was matched. In the definition of the Sauter mean diameter N_i is the number count of particles with fractional diameter d_i.

Following the existing concept of transport-based rCFD, we distilled these simulations into databases consisting of time frames of (Lagrangian) cell-to-cell shift patterns together with (Eulerian) fields of volume fraction of the bulk solid phase. Note that at this point any information of individual particles was lost such that the available data was strictly linked to the (Eulerian) computational grid.

In a second data-extrapolation phase, we aim to trace individual particle fractions on the cell-to-cell shift patterns of the joint solid phase. Without any relative drift, this would resemble the propagation of a species concentration on the bulk solid-phase. However, in contrast to molecular species, individual particle fractions exhibit different convective shift patterns than the corresponding bulk solid-phase. In an attempt to quantify these differences, we propose a fractional velocity decomposition,

$$\boldsymbol{u}_i = \boldsymbol{u}_s + \boldsymbol{u}_{d,i} = \boldsymbol{u}_s + \mathrm{u}_{d,i}\boldsymbol{e}_z \tag{1}$$

with $\boldsymbol{u}_i$ as the velocity of an individual particle fraction, which differs from the velocity of the bulk solid-phase, $\boldsymbol{u}_s$, by a fractional drift velocity, $\boldsymbol{u}_{d,i}$. Furthermore, we boldly assume that any particle drift just occurs in vertical direction (expressed by unit vector $\boldsymbol{e}_z$), thus aligned with the main direction of the supporting gas flow.

Finally, we have to define the directional (scalar) drift velocity $\mathrm{u}_{d,i}$ for a given particle fraction. Assuming that size-dependent particle segregation originates from differences in gas-particle drag force, we set

$$\mathrm{u}_{d,i} \sim \left(f_{drag,i} - f_{drag,32}\right) \tag{2}$$

with $f_{drag,i}$ being the drag force of a homogeneous cloud of particles with diameter d_i and $f_{drag,32}$ representing the corresponding drag force for a cloud of Sauter mean particles at the same solid volume fraction. Since $f_{drag,i}$ scales with particle area, i.e. the square of the diameter, we deduce that

$$\mathrm{u}_{d,i} \sim \left(d_i^2 - d_{32}^2\right), \tag{3}$$

with d_i and d_{32} being the fractional and Sauter mean diameter respectively. Considering this square dependency, we propose two alternative correlations for the fractional drift velocity,

$$\mathrm{u}_{d,i,A} = -k_{d,A}\left(d_i^2 - d_{32}^2\right) \tag{4}$$

as well as

$$\mathrm{u}_{d,i,B} = -k_{d,B}(d_i - d_{32})|d_i - d_{32}| \tag{5}$$

In both cases an empirical constant k_d is introduced, which has to be determined by numerical calibration (as discussed further below). Furthermore, note that for small particles the fractional drift velocity $\mathrm{u}_{d,i}$ points upward towards the freeboard and while it points downward towards the bottom of the bed for large particles.

Some attempts at obtaining estimates for the constant k_d have been made, for instance considering the correlations for the momentum exchange between solid fractions used in continuous TFM simulations, but it was impossible to create a robust procedure that guarantees good results in all regimes we considered. However, as a first step, it is still worth asking whether a model as simple as that in equation (5) is enough to describe polydisperse segregation, including a single free parameter.

In principle, one could also model the local fractional drift velocity as a more general function $\boldsymbol{u}_{d,i} = \boldsymbol{u}_{d,i}\left(d_i, d_{32}, \boldsymbol{u}_s, \boldsymbol{u}_g\right)$ including the solid and gas velocities. One might either investigate different ansatz functions with a small number of tuning parameters or use detailed CFD-DEM data to train a simple feed-forward neural network to predict the drift. However, this study demonstrates that even with a very simple correlation, it is possible to simulate segregation effects with rCFD with acceptable accuracy.

2.2.2. Numerical implementation

We employ the same computational domain and the same grid in rCFD and standard CFD-DEM simulations. In principle, a certain degree

of coarsening may be compatible with our model, but it is not introduced in this study, for the sake of simplicity.

From an algorithmic viewpoint, transport-based rCFD relies on two types of discrete transport operators – namely cell-to-cell shifts and face swaps. In principle, both operators could be adapted in order to account for drifting particle fractions. However, arranging for dedicated fractional cell-to-cell shift pattern would inevitably lead to multiple databases which might render impractical for poly-disperse particle ensembles.

Therefore, we opted for considering drifting particle fractions by directional face swaps. Within one swap operation a given cell receives a mass of

$$\mathrm{m}_{di} = c_{di}\alpha_s\rho_s(u_{di}A_{z\perp}\Delta t_{rec}) \tag{6}$$

fractional particles from a vertically neighbouring sending cell. In the equation above, c_{di} represents the mass concentration of fractional particles and α_s is the bulk solid volume fraction in the sending cell, ρ_s is the particle density, u_{di} is the scalar fractional drift velocity, $A_{z\perp}$ is the horizontally projected face area and Δt_{rec} is the recurrence time-step width. Note that for $u_{di} > 0$ (representing small particles) the sending cell will be the lower cell and vice versa.

While this equation is very simple, its implementation in the (MPI parallel) framework of rCFD provided some challenges. Especially for large drift velocities the mass of face-swapped particles might exceed the available amount of particles in the sending cell. In order to account for such cases, we introduced adaptive sub-iterations (with smaller time-step widths), such that particles can drift across more than one cell during a time-span of Δt_{rec}.

2.2.3. Model assumptions

Before proceeding with first results it might be valuable to recap our main mode assumptions.

First, we only consider size dependent particle segregation which is governed by differing gas–solid drag forces. While a similar strategy could be used for density-dependent segregation, it would take significantly more effort to picture, e.g., percolation effects in dense beds. One would have to regress the relative velocity of smaller grains depending on the local bed composition and dynamics from detailed DEM calculations, which should be possible given a sufficient amount of data but goes beyond the scope of our present investigation.

Furthermore, we assume that local segregation is aligned with the main direction of gas flow, which in our quasi-2D bed coincides with the vertical axis. This might pose problems in tapered or conical fluidized beds, where the direction of segregation would have to be aligned to the direction of local gas flow.

Next, the proposed model for the local fractional drift velocity introduces an empirical constant k_d, which has to be calibrated before this model can be applied. While sophisticated calibration routines exist, we opted for manually tuning the value of k_d by comparing rCFD predictions with the four database CFD-DEM simulations (see Fig. 2, further details are given in the next section).

Finally, we accept our CFD-DEM simulations as the numerical ground-truth for the validation of rCFD simulations. This is further substantiated by the fact that the used CFD and DEM model parameters had been calibrated by real-world materials (Diez et al., 2019) and equivalent CFD-DEM simulations on segregation had been validated by corresponding experiments in our previous publication (Atxutegi et al., 2024).

3. Results

3.1. Segregation in bi-disperse fluidized beds

As a first test case, we considered incipient segregation in a bi-disperse bubbling fluidized bed.

In order to give a first impression on how rCFD simulations predict time-evolving segregation Fig. 1 provides contour plots of the fractional volume fraction at three instances of time. Starting from a nearly perfectly mixed bed at $t = 1$s, a layer of large particles is formed at the bottom of the bed, while a corresponding accumulation of smaller particles can be observed in the upper fountain region of the bed (in Fig. 1 this is indicated by black and white arrows).

For a quantitative assessment of rCFD simulations, we compared these predictions to corresponding full CFD-DEM simulations. This comparison is further used to calibrate the rCFD's model parameters k_d. For this purpose, we considered four cases by varying the particle population (rows in Fig. 2) as well as the superficial gas velocity (columns in Fig. 2). All cases share the same Sauter mean diameter of the bed inventory.

Quite intuitively, macroscopic segregation can be characterized by plotting the time-evolution of the mean vertical coordinate of a given particle fraction. Fig. 2 depicts corresponding results from particle-based CFD-DEM simulations (black lines). After the artificial collapse of the initial loose particle arrangement a bubbling bed motion starts as indicated by the bed's vertical center of gravity (solid black line). Actually, the mean vertical coordinates of the two particle fractions differ from that line such that the dashed line of the large particle fraction becomes lower and the dotted line of the small particles becomes higher. Obviously, this representation provides an intuitive characterization of particle segregation. Based on these four cases we can conclude that segregation is more pronounced for wide PSDs (bottom row in Fig. 2) and further that segregation occurs slightly faster with more gas agitation (right column in Fig. 2).

In order to calibrate the empirical model parameter k_d, we applied our novel rCFD in pure replay mode. In this calibration mode, rCFD just reruns the frames in the database in their given order. Notably, this entails that the time-evolution of the bed's center of gravity is predefined and only the deviations thereof are results of rCFD simulations. Any deviation between rCFD predictions and the CFD-DEM based ground-truth is quantified by the error

$$\Delta_{seg} = \frac{\left(\overline{z_{CoG,s} - z_{CoG,l}}\right)\big|_{rCFD} - \left(\overline{z_{CoG,s} - z_{CoG,l}}\right)\big|_{CFD-DEM}}{\left(\overline{z_{CoG,s} - z_{CoG,l}}\right)\big|_{CFD-DEM}} \bullet 100\% \tag{7}$$

with $\left(z_{CoG,s} - z_{CoG,l}\right)$ being the difference between the vertical center-of-gravity coordinate of the small and large particle fraction and the superbar indicating time averaging, which we in this case applied only for the last second (i.e. between 4 s and 5 s). After manually tuning our empirical model parameter k_d we obtained two candidates for $k_{d,A}$ and $k_{d,B}$ with acceptable deviations given in Table 4.

Generally, it can be noted that rCFD predictions of segregation agree very well for the narrow particle diameter pairing while some deviations exist for the wide diameter pairing. At this point, we accepted these deviations and proceeded with the empirical model parameter of $k_{d,B} = 5e3$ [1/ms] and the drift velocity correlation given in equation (5).

After calibration we augmented Fig. 2 by rCFD predictions of particle segregation (red lines) which agree quite well with the corresponding CFD-DEM simulations. Given the simplicity of the proposed model, these results are both surprising and encouraging.

In a next test, we switched to the normal rCFD mode of data-assisted time-extrapolation. In this mode, rCFD relies on a restricted database representing only a short duration of time. Beyond that time-span, rCFD time-extrapolates recurrent flow pattern by stitching sequences of frames from the database. In our specific case we deduce our databases for a duration of 1.5 s and we furthermore start recording the data at a simulation time of 3 s in order to avoid any spin-up abnormalities. In Fig. 3 stitching-mode rCFD predictions of time-evolving segregation are depicted together with corresponding CFD-DEM results. In this representation segregation is expressed by the difference between the vertical center of gravity coordinates of the small and large particles, $\Delta\langle z\rangle$. Obviously, in the stitching mode rCFD predictions of the fractional

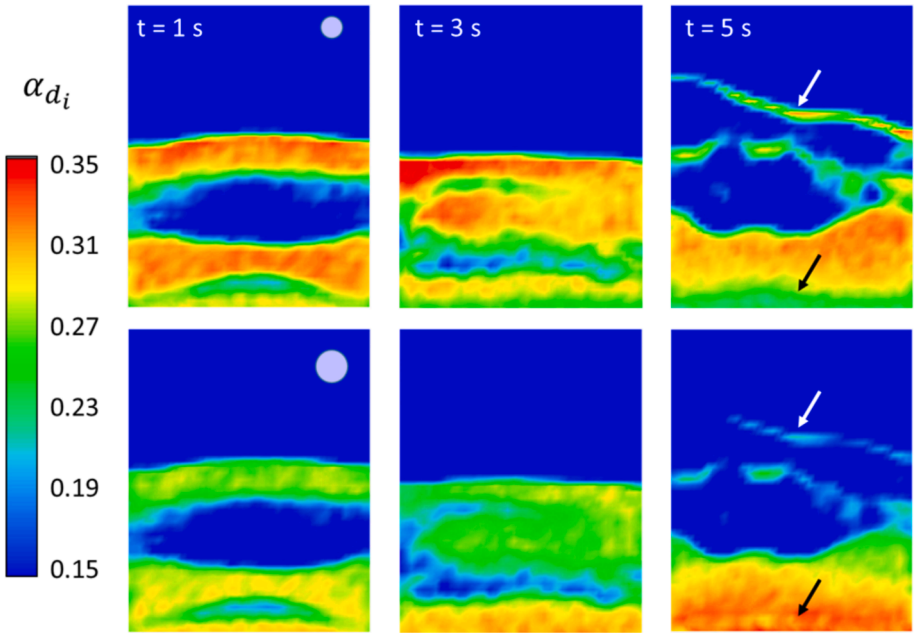

Fig. 1. Fractional volume fraction α_{d_i} as result of rCFD simulations at three instances of time evaluated for small particles (upper row) and large particles (lower row); white arrows indicate accumulation of small particles in the fountain region while black arrows indicate accumulation of large particles in the bottom region.

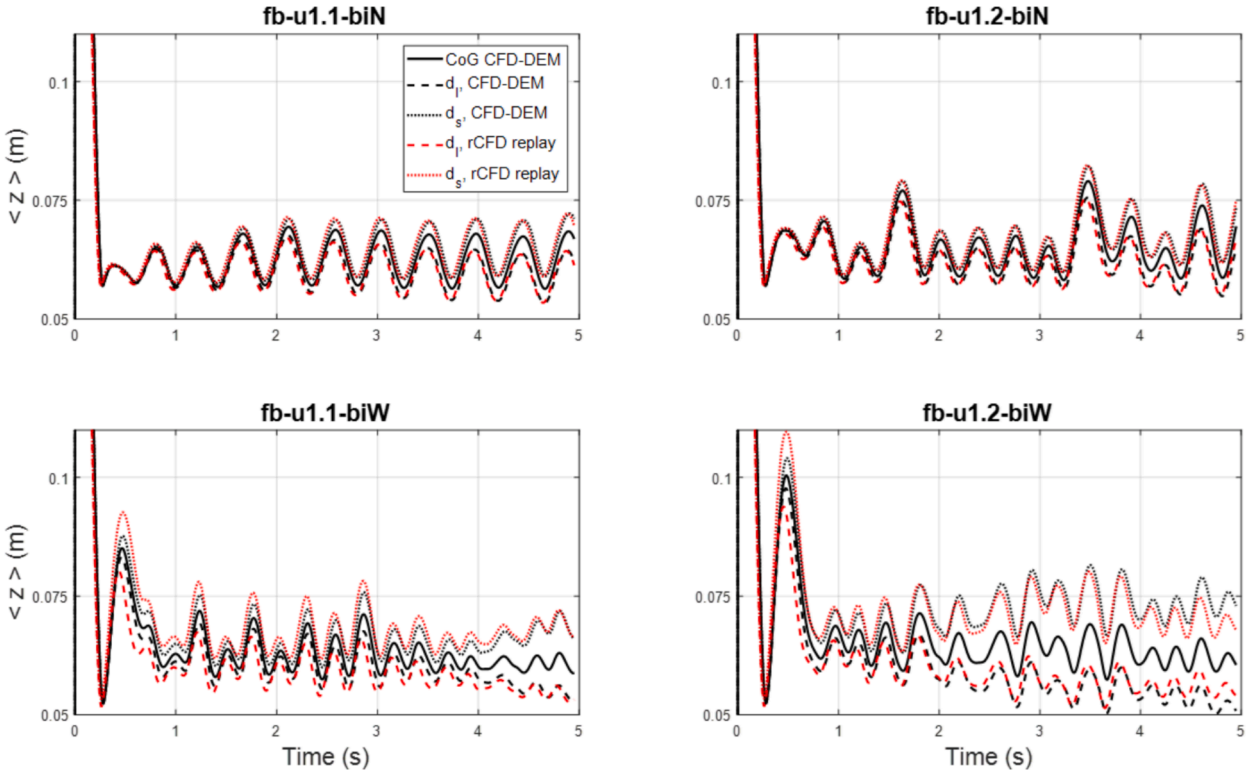

Fig. 2. Particle-based CFD-DEM simulations (black) and rCFD simulations in replay mode (red) of center-of-gravity vertical coordinate of the total bed (solid line) as well as large particles (dashed line) and small particles (dotted line); the four cases feature small and medium superficial gas velocity (left and right column) as well as narrow and wide particle size distributions (top and bottom rows), case names refer to Table 2. (For interpretation of the references to colour in this figure legend, the reader is referred to the web version of this article.)

center of gravity lines exhibit unnatural jumps due to data sequence stitching and a one-to-one comparison is not possible anymore. Even so the time-evolution of segregation is predicted fairly well at least in terms of magnitude. In just another representation, vertical profiles of fractional volume fraction are given in Fig. 4. In order to assess these profiles, we applied time averaging for 1 s (in between 4 s and 5 s) as well as spatial averaging across the bed depth. In all cases, these profiles highlight particle-size dependent segregation. Especially for the case of a large diameter ratio we further see a dominant accumulation of large particles at the bottom of the bed. This might be an indication for future

Table 4
Deviations between segregation predictions by rCFD and CFD-DEM, positive values indicate that rCFD over-predicts segregation (and vice-versa); case names indicate superficial gas velocity and particle population as defined in Table 2.

k_d [1/ms]	fb_u1.1_biN	fb_u1.2_biN	fb_u1.1_biW	fb_u1.2_biW
$k_{d,A} = 5e2$	$\Delta_{seg} = 8.7$ %	4.4	−36.1	−57.0
$k_{d,B} = 5e3$	−0.2	−3.2	19.0	−27.6

de-fluidization as we will discuss in the next section. Overall, predictions from rCFD simulations once again seem to agree fairly well with those from CFD-DEM reference simulations.

3.2. Long-term segregation and potential de-fluidization

In this section we prolonged our rCFD simulation and compared the results to expensive long-term CFD-DEM reference simulations (just run for the purpose of validation).

This time, we focused our post-processing on the bottom layer of the fluidized bed thus questioning the potential occurrence of de-fluidization. In Fig. 5 the time evolution of the Sauter mean diameter in a bottom neighbouring cell layer is given in the top row. Note that this time our four cases are arranged differently with both superficial velocities of the narrow PSD in the left column and those of the wide PSD in the right column.

In all cases, rCFD predictions show an initial rise of this bottom layer Sauter mean diameter above the mean Sauter diameter of the whole bed inventory which is given by the black line, indicating an accumulation of large particles close to the bottom of the fluidized bed. However, this predicted fractional particle redistribution levels out after about 5 s.

In a second post-processing step, we translated this local Sauter diameter into a minimum fluidization velocity using a correlation from

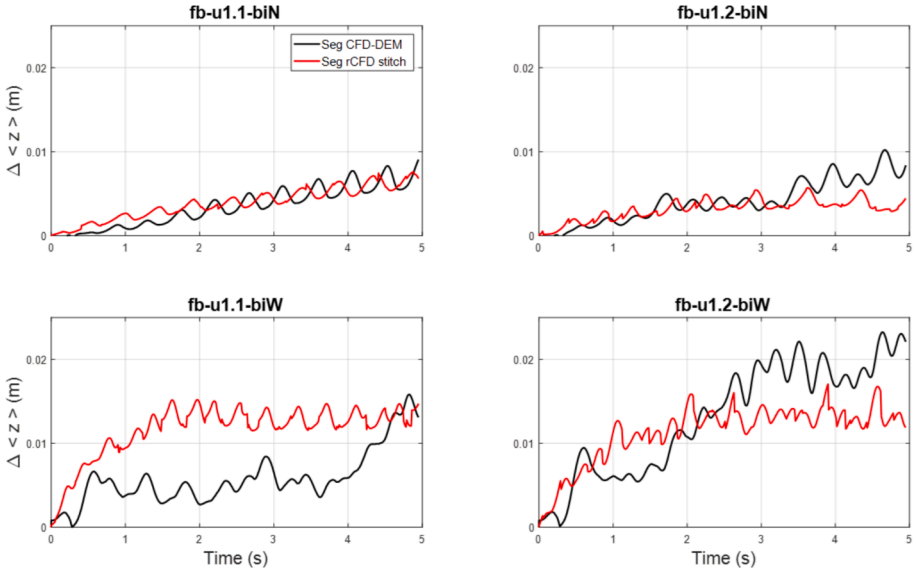

Fig. 3. Particle resolved CFD-DEM simulations (black lines) and rCFD simulations in stitching mode (red lines) of center-of-gravity z-coordinate difference between large and small particle fractions. (For interpretation of the references to colour in this figure legend, the reader is referred to the web version of this article.)

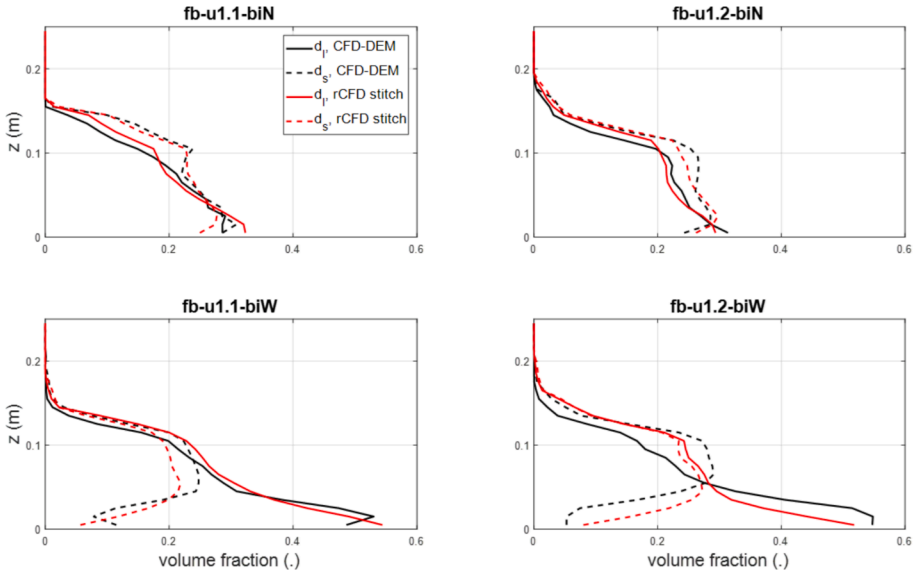

Fig. 4. Vertical profiles of temporal and spatially averaged profiles of particle volume fraction as result of full CFD-DEM simulations (black) and rCFD simulations (red) representing large particles (solid lines) and small particles (dashed lines); the four cases are the same as in the previous Figures. (For interpretation of the references to colour in this figure legend, the reader is referred to the web version of this article.)

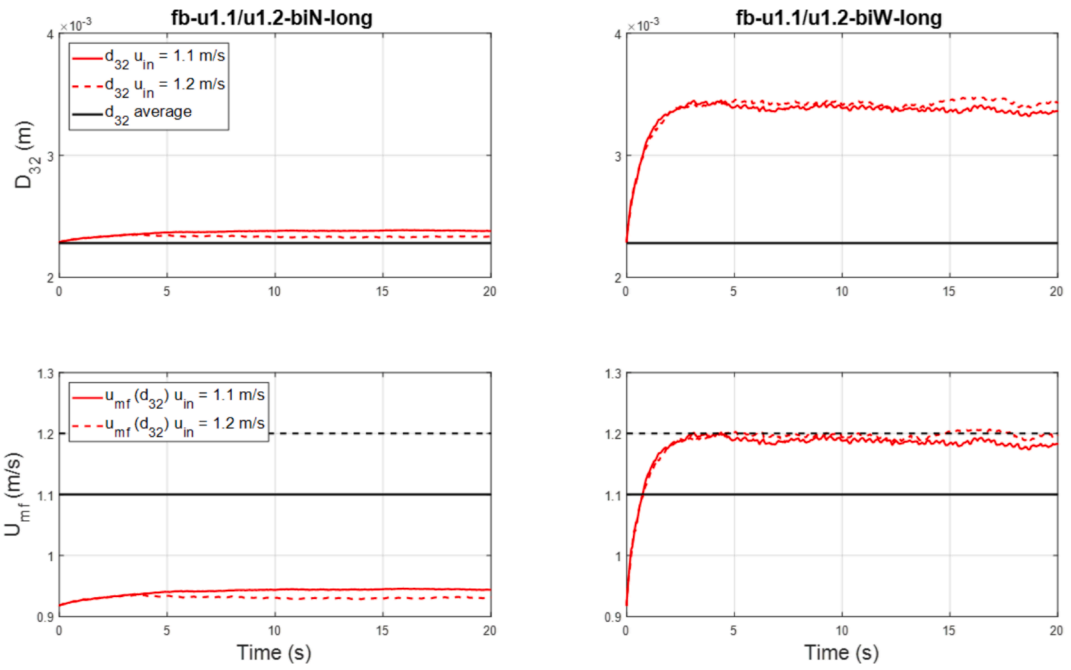

Fig. 5. Time evolution of bottom-layer Sauter mean diameter (top) and corresponding estimation of minimum fluidization velocity (bottom) for narrow (left) and wide (right) PSDs as result of rCFD simulations; the black lines in the top Figures represent the Sauter mean diameter of the total bed inventory while the red lines in the bottom Figures represent the considered low (solid line) and high (dashed line) minimum fluidization velocities and the horizontal black lines indicate the cases' superficial gas velocities. (For interpretation of the references to colour in this figure legend, the reader is referred to the web version of this article.)

literature (equation (7) in Shao et al. (2019); note that minimum fluidization depends on the Sauter mean diameter in a slightly non-linear fashion). In the bottom row of Fig. 5, the time-evolution of minimum fluidization velocity for the bottom layer is depicted by red lines. For the case of the narrow PSD (left side in Fig. 5), the required minimum fluidization velocity is clearly below the superficial velocity as required for continuous fluidization. In contrast to that, the minimum fluidization velocities of the wide PSD cross the lower superficial gas velocity indicating that in that case de-fluidization will potentially occur after only 3 s. Also for the case of the higher gas velocity, the estimated minimum fluidization velocity quickly approaches the velocity of the supporting gas, eventually crossing it at about 16 s. While this exact instance of time is questionable and certainly depends on the chosen correlation for the minimum fluidization velocity, our long-term rCFD simulations clearly provide an indication that the cases with wide PSD might be prone to de-fluidization.

In corresponding long-term CFD-DEM reference simulations, we had access to the mobility of individual particles and hence could directly detect the onset of de-fluidization. In Table 5 the percentage of immobile particles is given at four instances of time. While for the narrow PSD no de-fluidization was observed at all, immobile particles were detected for the wide PSD, especially in case of low superficial gas velocity. In the latter case, as much as a tenth of the total particle mass just resided on the bottom of the bed at a simulation time of 20 s. From a qualitative perspective, this agrees well with our rCFD indications. This perhaps surprising result can intuitively be explained by the fact that de-fluidization is inextricably linked with pronounced segregation. Despite its simplicity, the drift velocity model results in deposition of the larger particles in the lower portion of the bed, eventually reaching a sufficient volume fraction to become immobile and thus leading to de-fluidization, as in the reference CFD-DEM simulation.

Table 5
Percentage of immobile particles as result of CFD-DEM simulations at four instances of time); case names indicate superficial gas velocity and particle population as defined in Table 2.

Case name	c_{im} [wt%] after 5/10/15/20 s
fb_u1.1_biN_long	0/0/0/0
fb_u1.2_biN_long	0/0/0/0
fb_u1.1_biW_long	0/0/6/10
fb_u1.2_biW_long	0/0/0/1

3.3. Segregation in penta-disperse fluidized beds

In a next step, we still relied on the databases we obtained previously by CFD-DEM simulations of a bi-disperse bed inventory, but this time we extrapolated our rCFD towards a penta-disperse particle mixture, which resembled the same Sauter mean diameter. Also in this case, full CFD-DEM simulations were performed just for the purpose of validating rCFD predictions.

As in the previous subsection, we sticked to our four cases while this time we opted to plot particle size distributions for the characterization of segregation. In Fig. 6 the time averaged (averaging again between 4 s and 5 s) PSD is given for the lower and the upper half of the fluidized bed. The slight tilt angle between the PSDs indicates segregation. This time, the agreement between rCFD simulations and corresponding CFD-DEM simulations is mixed. While it is excellent for two cases (top left and bottom right), it significantly deviates for the other two cases (top right and bottom left).

In an attempt to explain these deviations, we compared the corresponding macroscopic bed dynamics as displayed by full CFD-DEM simulations for bi-disperse and penta-disperse simulations with the same Sauter mean diameter. As a metrics for the dynamics of the bubbling fluidized bed, we define the mean deviation of bed height $\Delta z_{CoG} = \overline{(z_{CoG} - \overline{z_{CoG}})}$ with z_{CoG} being the instantaneous vertical Center-of-Gravity (CoG) coordinate of the bed and the superscript bar indicating time averaging. After calculating Δz_{CoG} for our four cases (two gas velocities and two PSDs) and both (bi- and penta-disperse) solid inventories, we can evaluate how essential the bed dynamics change upon switching from bi-disperse to penta-disperse bed inventories. For quantitative comparison we further defined a database distance by $\Delta DB = \left(1 - \left|\Delta z_{CoG,penta} - \Delta z_{CoG,bi}\right|\right) \bullet 100\%$. The resulting distance

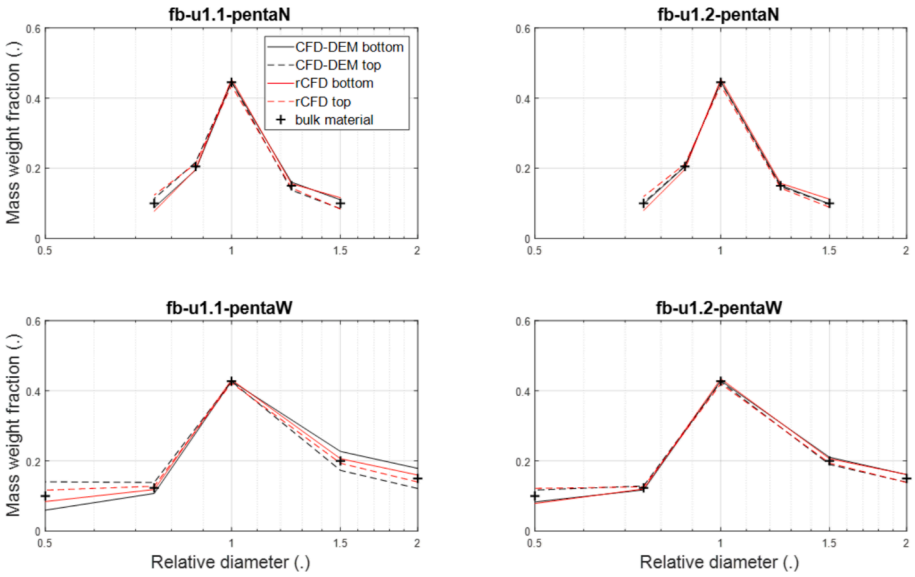

Fig. 6. Particle size distributions in bottom half (solid lines) and top half (dashed lines) of the fluidized bed as result of CFD-DEM simulations (black lines) and rCFD simulations (red lines); relative diameter relates to the Sauter mean diameter; case names refer to Table 2. (For interpretation of the references to colour in this figure legend, the reader is referred to the web version of this article.)

values given in Table 6 allow for a very clear conclusion. While in two cases agreement was very good (with ΔDB values below 10 %), the dynamic bed behaviour obviously changed significantly for the other two cases (with ΔDB values of 26 % and even 230 %). In the latter cases our penta-disperse rCFD simulation just relied on a wrong dynamic state. It is as simple as this: If the database is wrong, rCFD is wrong!

This finding highlights a conceptual dilemma of rCFD. Obviously, particle segregation is governed by fluid flow. However, particle segregation cannot be considered as perfectly passive – rather it also back-influences the flow dynamics in return. Hence, we would have to update the underlying database. While small database deviations might be negligible, an update becomes mandatory for larger deviations. Unfortunately, we have no easy means of evaluating database deviations on the fly, i.e. in the course of a rCFD simulation. In order to assess the validity of the database, we have to switch back to full CFD-DEM simulation and monitor Δz_{CoG}. In case it differs significantly from the old database, we would have to create a new one. While this procedure should be possible, we abstain from implementing multiple databases into rCFD in order not to overload this paper.

3.4. Particle growth and particle through-flow

In this section we aim to prove the feasibility of incorporating particle growth and particle through-flow into poly-disperse rCFD simulations. For this purpose, we sticked to our quasi-2d bed geometry and just defined three sub-regions accounting for a spray zone (in a middle top region) as well as two side zones (in two opposite side-bottom regions, mimicking weir underflows) for the inflow and outflow of particles.

In our simplified spray zone, we assumed a constant global granulation rate $\dot{m}_g = \sum_i \dot{m}_{g,i} = const$, with $\dot{m}_{g,i}$ representing the granulation rate of an individual particle fraction. Thereby, the share of the global granulation rate to the individual particle fractions relates to their respective projected particle areas, $\dot{m}_{g,i}/\dot{m}_{g,j} = N_{di} d_i^2 / N_{dj} d_j^2$, with $N_{di,j}$ being the local number of particles with diameter $d_{i,j}$. Finally, a fixed portion of $\dot{m}_{g,i}$ will lead to a local mass loss of particle fraction i and a corresponding mass gain of the larger particle fraction by $\dot{m}_{g,i\to i+1} = c\dot{m}_{g,i}$ with $c = 0.01$ as empirical constant. While certainly more sophisticated models for granulation exist, we accepted these simplifications at the moment for the sake of brevity.

In Fig. 7 the black symbols indicate the initial PSD of the solid inventory. Without considering particle growth and particle through-flow, rCFD simulations in this setting predict only mild segregation as depicted by the upper and lower PSDs (black lines in Fig. 7). If we repeat this simulation with particle growth, we obtain the red PSDs (left side of Fig. 7). Obviously, our granulation kernel shifts the PSDs towards larger particle fractions, leading to a depletion of small particles and an accumulation of larger particles (in Fig. 7 this is indicated by red arrows). Without counter measures this would inevitably lead to severe segregation and subsequent de-fluidization.

Steady-state granulation processes can only operate in combination with continuous inflow of small particles and continuous extraction of the larger granulated product. In our feasibility study we modelled continuous in- and outflow by a total through-flow rate $\dot{m}_{tf} = \sum_i \dot{m}_{i,in} = \sum_i \dot{m}_{i,out}$, where the individual fractional inflow rates were defined by the initial bed inventory, $\dot{m}_{i,in}/\dot{m}_{j,in} = m_{i,0}/m_{j,0}$, and the outflowing mass related to the local fractional concentrations, $\dot{m}_{i,out}/\dot{m}_{j,out} = c_i/c_j$.

By employing continuous particle feed and product extraction a steady state granulation process could be achieved as represented by blue PSDs (right side of Fig. 7; the stabilizing effect of continuous through-flow is indicated by blue arrows).

Table 6
Difference in dynamic bed behaviour as result of bi- and penta-disperse CFD-DEM simulations.

Case names	ΔDB [%]
fb_u1.1_biN/fb_u1.1_pentaN	8
fb_u1.2_biN/fb_u1.2_pentaN	26
fb_u1.1_biW/fb_u1.1_pentaW	231
fb_u1.2_biW/fb_u1.2_pentaW	8

3.5. Computational efficiency

It is well known that full CFD-DEM simulations are very expensive by means of computational resources. Considering a penta-disperse bed inventory is even more expensive due to the excess number of small particles and the unfavourably large neighbour lists needed for poly-disperse particle ensembles (note that we did not use a hierarchical grid for acceleration). In Table 7 corresponding CFD-DEM run times are given for two representative bi- and penta-disperse cases. In that case simulations were run in parallel on four partitions on a (rather old)

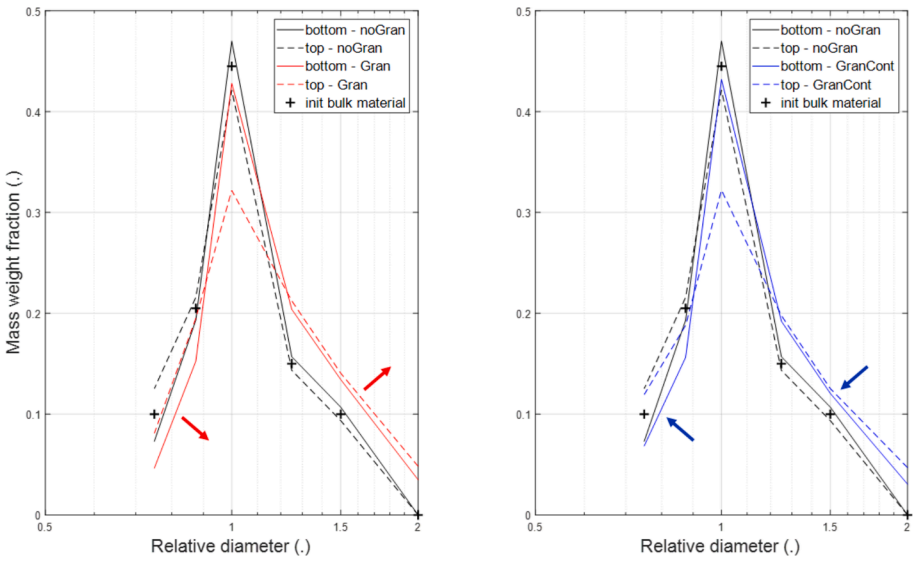

Fig. 7. Particle size distribution in the bottom half (solid lines) and top half (dashed lines) of the fluidized bed as result of rCFD simulations with neither particle growth nor particle through-flow (black lines), with particle growth but without particle through-flow (red lines, left) and with both (blue lines, right); blue arrows indicate how continuous through-flow stabilized the particle population. (For interpretation of the references to colour in this figure legend, the reader is referred to the web version of this article.)

Linux cluster.

In contrast to this, rCFD simulations run in the same order as the real-world process. Based on the same partitioning and run on the same hardware as the CFD-DEM simulations, rCFD took just 4 s to 7 s to cover 1 s of real-world process time. Note that this time refers to the pure run time, thus excluding the effort needed for establishing and loading the database.

Given its general real-time capability, we could think about running rCFD simulations concurrently to the actual real world process (Pirker & Lichtenegger, 2019). In case of granulation, such digital twin simulations could provide additional information on bed heterogeneities (e.g. fluctuations in product PSD or the likeliness of de-fluidization).

4. Conclusion and outlook

In this study we further developed recurrence CFD (rCFD) in order to account for segregating particle fractions in bubbling fluidized beds.

Despite the simplicity of the proposed approach, we obtained good agreement with full particle-based CFD-DEM simulations in terms of macroscopic segregation (expressed by the time-evolution of the fractional centre-of-gravity coordinates) as well as for vertical profiles of fractional particle volume fraction. At the same time rCFD simulations were more than four orders of magnitude faster than corresponding CFD-DEM simulations.

Focusing on the evolution of the local Sauter mean diameter in a bottom layer of the bed, we further estimated a local minimum fluidization velocity, which together with the superficial gas velocity can indicate potential de-fluidization in qualitative agreement with long-term CFD-DEM simulations.

Next, we tried to extrapolate bi-disperse databases towards penta-disperse bed inventories. We could show that this works as long as the underlying bed-dynamics is not significantly changed by switching the bed inventory. This clearly highlights an existing limitation of poly-disperse rCFD simulations. Future work will therefore be dedicated to the incorporation of multiple databases for the case of changing bed dynamics.

Finally, we proved the feasibility of rCFD simulations of a granulation chamber featuring particle growth and particle through-flow and sketched the future perspective of running such rCFD simulations as real-time capable digital twins concurrently to the real-world process.

Table 7
Computational time needed for the simulation of one second of real-world process time; all simulations were run in parallel at four partitions on the same Linux cluster.

case name	compute time for 1 s process time [s]/[h]	
fb_u1.1_biN	CFD-DEM	59 138/16
	rCFD	4/0
fb_u1.1_pentaW	CFD-DEM	79 975/22
	rCFD	7/0

In the present study, we focused on a relatively simple bed configuration, which was enough to observe the occurrence of segregation but where the choice of the main direction of the gas flow was obvious. A generalization for more complex fluidized beds, where the direction of the drift velocity is local, will be necessary. Finally, it is important to note that our model is not capable of describing segregation that occurs in densely packed beds, where it is caused by percolation rather than by a different balance between gravity and drag force.

CRediT authorship contribution statement

S. Pirker: Writing – original draft, Visualization, Validation, Software, Methodology, Funding acquisition, Conceptualization. **M. Atzori:** Software, Methodology, Data curation. **S. Heinrich:** Writing – review & editing, Funding acquisition. **T. Lichtenegger:** Writing – review & editing, Supervision, Project administration, Methodology, Conceptualization.

Declaration of competing interest

The authors declare that they have no known competing financial interests or personal relationships that could have appeared to influence the work reported in this paper.

Acknowledgments

The authors acknowledge the financial support of the Austrian Science Fund (FWF), project number I-5180-N, as well as the German Research Foundation (DFG), project number HE 4526/31-1.

Data availability

Data will be made available on request.

References

Atxutegi, A., Atzori, M., Bettien, J., Lichtenegger, T., Puttinger, S., Pirker, S., Heinrich, S., 2024. Control of segregation by non-uniform aeration in a fluidized bed spray granulator. *Powder Technol.* 435. https://doi.org/10.1016/j.powtec.2023.119348.

CFDEMcoupling PFM. (2024). https://github.com/ParticulateFlow/CFDEMcoupling-PFM.

Chew, J.W., LaMarche, W.C.Q., Cocco, R.A., 2022. 100 years of scaling up fluidized bed and circulating fluidized bed reactors. *Powder Technol.* 409. https://doi.org/10.1016/j.powtec.2022.117813.

Dabbagh, F., Pirker, S., & Schneiderbauer, S. (2020). On the fast modeling of species transport in fluidized beds using recurrence computational fluid dynamics. *AIChE J.*, *January*, 1–20. 10.1002/aic.16931.

Dahl, S.R., Hrenya, C.M., 2005. Size segregation in gas-solid fluidized beds with continuous size distributions. *Chem. Eng. Sci.* 60 (23), 6658–6673. https://doi.org/10.1016/j.ces.2005.05.057.

de Munck, M.J.A., Dullemond, M., Peters, E.A.J.F., Kuipers, J.A.M., 2023. Experimental gas-fluidized bed drying study on the segregation and mixing dynamics for binary and ternary solids. *Chem. Eng. J.* 465. https://doi.org/10.1016/j.cej.2023.142756.

Diez, E., Kieckhefen, P., Meyer, K., Bück, A., Tsotsas, E., Heinrich, S., 2019. Particle dynamics in a multi-staged fluidized bed: Particle transport behavior on micro-scale by discrete particle modelling. *Adv. Powder Technol.* 30 (10), 2014–2031. https://doi.org/10.1016/j.apt.2019.05.025.

Fries, L., Antonyuk, S., Heinrich, S., Palzer, S., 2011. DEM-CFD modeling of a fluidized bed spray granulator. *Chem. Eng. Sci.* 66 (11), 2340–2355. https://doi.org/10.1016/j.ces.2011.02.038.

Jiang, Z., Hagemeier, T., Bück, A., Tsotsas, E., 2018. Color-PTV measurement and CFD-DEM simulation of the dynamics of poly-disperse particle systems in a pseudo-2D fluidized bed. *Chem. Eng. Sci.* 179, 115–132. https://doi.org/10.1016/j.ces.2018.01.013.

Joseph, G.G., Leboreiro, J., Hrenya, C.M., Stevens, A.R., 2007. Experimental segregation profiles in bubbling gas-fluidized beds. *AIChE J* 53 (11), 2804–2813. https://doi.org/10.1002/aic.11282.

Kieckhefen, P., Lichtenegger, T., Pietsch, S., Pirker, S., Heinrich, S., 2019. Simulation of spray coating in a spouted bed using recurrence CFD. *Particuology* 42, 92–103. https://doi.org/10.1016/j.partic.2018.01.008.

Lichtenegger, T., Kieckhefen, P., Heinrich, S., Pirker, S., 2019. Dynamics and long-time behavior of gas–solid flows on recurrent-transient backgrounds. *Chem. Eng. J.* 364 (January), 562–577. https://doi.org/10.1016/j.cej.2019.01.161.

Lichtenegger, T., Peters, E.A.J.F., Kuipers, J.A.M., Pirker, S., 2017. A recurrence CFD study of heat transfer in a fluidized bed. *Chem. Eng. Sci.* 172. https://doi.org/10.1016/j.ces.2017.06.022.

Lichtenegger, T., Pirker, S., 2016. Recurrence CFD – A novel approach to simulate multiphase flows with strongly separated time scales. *Chem. Eng. Sci.* 153. https://doi.org/10.1016/j.ces.2016.07.036.

Olaofe, O.O., Buist, K.A., Deen, N.G., van der Hoef, M.A., Kuipers, J.A.M., 2013. Improved digital image analysis technique for the evaluation of segregation in pseudo-2D beds. *Powder Technol.* 244, 61–74. https://doi.org/10.1016/j.powtec.2013.03.051.

Pirker, S., Lichtenegger, T., 2018. Efficient time-extrapolation of single- and multiphase simulations by transport based recurrence CFD (rCFD). *Chem. Eng. Sci.* 188. https://doi.org/10.1016/j.ces.2018.04.059.

Pirker, S., Lichtenegger, T., 2019. Process control of through-flow reactor operation by real-time recurrence CFD (rCFD) simulations – Proof of concept. *Chem. Eng. Sci.* 198. https://doi.org/10.1016/j.ces.2018.09.043.

Rowe, P.N., Nienow, A.W., 1976. Particle Mixing and Segregation in Gas Fluidised Beds. A Review*. *Powder Technol.* 15, 141–147.

Schneiderbauer, S., Puttinger, S., Pirker, S., 2015. Numerical study of a Bi-disperse gas-solid fluidized bed using an Eulerian and Lagrangian hybrid model. *Procedia Eng.* 102. https://doi.org/10.1016/j.proeng.2015.01.289.

Shao, Y., Gu, J., Zhong, W., Yu, A., 2019. Determination of minimum fluidization velocity in fluidized bed at elevated pressures and temperatures using CFD simulations. *Powder Technol.* 350, 81–90. https://doi.org/10.1016/j.powtec.2019.03.039.

Wiegel, D., Eckardt, G., Priese, F., Wolf, B., 2016. In-line particle size measurement and agglomeration detection of pellet fluidized bed coating by Spatial Filter Velocimetry. *Powder Technol.* 301, 261–267. https://doi.org/10.1016/j.powtec.2016.06.009.

Wu, S., Baeyens, J., 1998. Segregation by size difference in gas fluidized beds. *Powder Technol.* 98, 139–150.

Zafiryadis, F., Degn Jensen, A., Lin, W., Akoh Hove, E., Boberg Larsen, M., & Wu, H. (2023). Injection of gas–liquid jets into gas–solid fluidized beds: A review. In *Particuology* (Vol. 76, pp. 63–85). Elsevier B.V. 10.1016/j.partic.2022.08.014.